BMC Plant Biology

https://doi.org/10.1186/s12870-026-08893-0

Article in Press

Aeschynomene americana induces terminal bacteroid differentiation in *Bradyrhizobium* sp. USDA3516, a novel model for dalbergioid–rhizobium symbiosis

Received: 15 December 2025

Accepted: 28 April 2026

Published online: 25 May 2026

Cite this article as: Carlew T.S., Atherton Puri A.P., Shim A. *et al. Aeschynomene americana* induces terminal bacteroid differentiation in *Bradyrhizobium* sp. USDA3516, a novel model for dalbergioid–rhizobium symbiosis. *BMC Plant Biol* (2026). https://doi.org/10.1186/s12870-026-08893-0

T. Scott Carlew, Annika P. Atherton Puri, Ashley Shim, Camilo Parada Rojas, Riley A. Buchanan, Jeff H. Chang, Joel L. Sachs & Brittany J. Belin

Aeschynomene americana induces terminal bacteroid differentiation in *Bradyrhizobium* sp. USDA3516, a novel model for Dalbergioid-rhizobia symbiosis

T. Scott Carlew[1], Annika P. Atherton Puri[1], Ashley Shim[1], Camilo Parada Rojas[3], Riley A. Buchanan[3], Jeff H. Chang[3], Joel L. Sachs[4], Brittany J. Belin[1,2]

[1]Department of Embryology, Carnegie Science, Baltimore, MD 21218
[2]Department of Biology, Johns Hopkins University, Baltimore, MD 21218
[3]Department of Botany and Plant Pathology, Oregon State University, Corvallis, OR 97331
[4]Department of Ecology, Evolution, and Organismal Biology, UC Riverside, Riverside, CA 92521
* corresponding author: belin@carnegiescience.edu

Author ORCIDs:

- Jeff H. Chang: 0000-0002-1833-0695
- Joel L. Sachs: 0000-0002-0221-9247
- Brittany J. Belin: 0000-0002-1837-3214

Word counts: Introduction – 621; Results – 1,546; Materials & Methods – 1,369; Discussion - 696
Display items: Tables – 2; Figures – 6 color, 1 grayscale; Supplemental Tables – 1; Supplemental Figures - 9
Keywords: *Aeschynomene*, bacteroid differentiation, bradyrhizobia, Dalbergia, legume-rhizobia symbiosis

ABSTRACT

Background: The paradigms of legume-rhizobia symbiosis are derived primarily from conserved features of Inverted-Repeat Lacking Clade (IRLC) legumes and closely related species. The Dalbergioids diverged from the IRLC early in legume evolution and possess unique symbiotic features but few genetically tractable models. The small, diploid Dalbergioid *Aeschynomene americana* (American jointvetch) has promise as a genetic model for Dalbergioid-rhizobia symbiosis, yet only a few studies have examined its symbiotic properties.

Results: We examined the symbiont range of *A. americana* from central Florida and characterized a native *A. americana* nodule isolate, *Bradyrhizobium* sp. USDA3516. We find that *A. americana* forms effective symbioses with *Bradyrhizobium* sp. USDA3516, which is closely related to Thai *A. americana* symbiont *Bradyrhizobium* sp DOA9, and with symbionts from the Dalbergioids stylo and peanut. Interestingly, several strains that effectively nodulated *A. americana* exhibited branched bacteroid morphologies, but we found that branching was neither necessary nor sufficient for effective symbiosis.

Conclusions: Our study contradicts the prevailing view that bacteroid shape is a major determinant of symbiotic efficiency and presents the *A. americana-Bradyrhizobium* sp. USDA3516 interaction as an optimal model of *A. americana* symbiosis.

BACKGROUND

The Fabaceae or legume family of plants contains nearly 30,000 accepted species [1], and many of these species form mutualistic symbioses with nitrogen-fixing rhizobia. Studies of the legume-rhizobia symbiosis have focused on the Papilionoideae subfamily, which is commonly split into Inverted-Repeat Lacking Clade (IRLC) tribes and non-IRLC tribes based on presence of an inverted repeat region in their plastid genomes [2]. Legume genetic tools were developed first in IRLC and closely related non-IRLC species, and as a result, the paradigms for legume-rhizobia symbiotic mechanisms are derived from conserved features across these clades.

According to these paradigms, legume-rhizobia symbiosis is initiated by bacterial Nod factors, which induce development of infection threads and new meristem tissue in the root cortex. This meristem differentiates into nodule cells that are intracellularly infected by rhizobia, and internalized rhizobia in turn differentiate into bacteroids through a host-dependent process. In soybean, bacteroid differentiation is minimal and consists of upregulation of nitrogen fixation and metabolite exchange factors [3]. In *Medicago* and other host genera, a "terminal" bacteroid differentiation occurs and includes altered bacteroid morphology and increased endoreduplication. This terminal bacteroid differentiation is driven by host nodule-specific, cysteine-rich (NCR) peptides [4].

Dalbergioid legumes such as peanut, the world's second most important commercial legume by production volume [5], diverged from the IRLC ancestor early in Papilionoideae evolution (**Fig. 1A**). This tribe is known to have unique symbiotic features. Many Dalbergioid legumes do not require Nod factors to initiate symbiosis [6, 7], and bacterial infection occurs through cracks in the root epidermis rather than an infection thread [7-9]. Terminal differentiation of bacteroids does occur in Dalbergioids and is driven by host-produced peptides, but these peptides generally are longer and more anionic than IRLC NCR peptides [10-13]. Identifying the molecular mechanisms of these unique symbiotic features of the Dalbergioids is key to understanding legume-rhizobia symbiosis evolution.

Most genetic work in the Dalbergioids has been performed in the jointvetches (*Aeschynomene* spp.), a genus of semi-aquatic legumes that includes the species *A. afraspera*, *A. indica*, *A. evenia*, *A. fluminensis*, and *A. americana*. Of these, only the diploid species *A. evenia* has a fully assembled genome [14]. *A. americana* is also diploid and thus a promising alternative model for Dalbergioid genetics [15, 16], and it has commercial relevance as a cover crop and for rice paddy intercropping (**Fig. 1B**). Currently there are few studies on *A. americana* symbiosis. Prior work indicates that *A. americana* symbioses are infection thread-independent and that compatible symbionts (namely *Bradyrhizobium* sp. DOA9) encode genes for Nod factor production, are non-photosynthetic, and do not terminally differentiate [9, 17, 18].

Here, we examine the symbiotic compatibility of *A. americana* with a panel of rhizobium type strains, including the *A. americana* nodule isolate *Bradyrhizobium* sp. USDA3516 [19]. We affirm that *A. americana* is not compatible with photosynthetic *Bradyrhizobium* spp. and that its overall symbiont range is more like the Dalbergioids peanut and stylo. Contradicting earlier work, we do observe hallmarks of terminal bacteroid differentiation, including endoreduplication and altered bacteroid morphology; however, altered morphology was not observed in all productive strains. Sequencing of *Bradyrhizobium* sp. USDA3516, the most effective strain tested, indicates that this strain likely produces Nod factors and encodes the BclA protein involved in NCR import [20]. These findings suggest that production of NCRs to induce terminal bacteroid differentiation may be universal in the Dalbergioids and is thus an ancient symbiotic mechanism.

RESULTS

A. americana symbiont range

Previous work indicated that *A. americana* nodulation is Nod factor-dependent and that *A. americana* is not nodulated with photosynthetic *Bradyrhizobium* spp. [9]. To investigate its symbiont range more broadly, we inoculated *A. americana* from central Florida with a collection of 13 rhizobium type strains, as well as one native strain (*Bradyrhizobium* sp. USDA3516) that was isolated from root nodules of *A. americana* grown in the same region (full strain names are provided in **Table 1**). Type strains used included strains engaged in both Nod factor-dependent and Nod factor-independent symbiosis and were isolated from diverse hosts.

At 14 days post-inoculation, we quantified shoot height, nodule counts, nodule dry biomass, and acetylene reduction rates of plants inoculated with each strain (**Fig. 2**). Four strains provided robust benefits to *A. americana*, eliciting >10 nodules per plant on average, and had significantly higher nitrogenase activity than uninoculated control plants, including *B. stylosanthis*, *B. arachidis*, *Bradyrhizobium* sp. USDA3516, and *B. cajani*. One strain, *Sinorhizobium fredii* HH103, provided significant fixed nitrogen but formed relatively few nodules. *B. diazoefficiens* inoculation increased plant shoot heights but produced few, ineffective nodules, suggesting that the benefit is not strictly due to symbiotic nitrogen fixation.

None of the remaining strains conferred benefits to *A. americana*. *B. canariense* nodulated *A. americana* robustly, but these nodules did not fix significant nitrogen. *B. semiaridum*, *S. fredii* NGR234, and *B. brasilense* nodulated weakly but also were ineffective. None of the remaining strains formed nodules on *A. americana,* including *B.* sp. ORS285, *B.* BTAi1, *B. japonicum*, and *B. elkanii*.

A. americana nodule and bacteroid morphology

We next examined nodule morphology from *A. americana* inoculated with each strain that exhibited robust nodulation (at least 10 nodules/plant on average), including *B. stylosanthis*, *B. arachidis*, *Bradyrhizobium* sp. USDA3516, *B. cajani*, and *B. canariense*. We collected semi-thin sections of nodules harvested at 14 days post inoculation (dpi), stained the sections with Calcofluor and the BacLight LIVE/DEAD kit, and imaged them by confocal microscopy. Interestingly, bacteroids of all strains except for *B. cajani* appeared to have morphological changes relative to typical free-living *Bradyrhizobium* spp. (**Fig. 3**). Nodules containing *Bradyrhizobium* sp. USDA3516 had much larger bacteroid volumes and branched bacteroid morphologies, whereas more subtle bacteroid morphological changes occurred in nodules with *B. stylosanthis*, *B. arachidis*, and the inefficient fixer *B. canariense*. We initially hypothesized that the variation in presence of morphological changes in bacteroids across strains was due to some strains requiring longer time windows to complete differentiation. However, nodules harvested at 35 dpi had similar bacteroid morphologies to the 14 dpi time point (**Fig. S1**).

To obtain more quantitative information on bacteroid characteristics, we isolated bacteroids from root nodules and compared them to free-living cells by imaging and flow cytometry (**Fig. 4**; **Fig. S2-S6**). In all strains, free-living cell morphologies were similar, exhibiting rod shapes of 3-6 microns length and 1-2 SYTO9 (DNA) foci in the cytoplasmic interior. Staining with the Nile Red (NR) dye under PHB granule-detecting conditions demonstrated that the free-living cells usually had few or no PHB granules. Bacteroid morphologies, however, were diverse across strains. In native symbiont *Bradyrhizobium* sp. USDA3516 (**Fig. 4A**; **Fig. S2**), extracted bacteroids had a branched

morphology and were slightly wider than free-living cells. Most bacteroids had multiple PHB granules and SYTO9 was either strong throughout the cytoplasm or present in multiple bright, discrete foci at the poles. The increased volume of *Bradyrhizobium* sp. USDA3516 bacteroids was clearly illustrated by forward scatter flow cytometry, and SYTO9 flow cytometry indicated that bacteroids had a higher ploidy than free-living cells, with a ~20% increase in median SYTO9 fluorescence. Bacteroids of *B. stylosanthis* were similar to *Bradyrhizobium* sp. USDA3516, albeit with a slightly higher increase (40%) in median SYTO9 signal (**Fig. 4D**; **Fig. S6**). We verified that the apparent branched morphologies and larger areas of *B. stylosanthis* and *Bradyrhizobium* sp. USDA3516 bacteroids were not due to clumping of multiple cells with the membrane dye FM 4-64, which revealed that branched bacteroids were surrounded by one continuous cell envelope (**Fig. S7-8**).

Differentiation of other strains was more variable. *B. arachidis* also formed mostly branched bacteroids with increased SYTO9 signals relative to free-living cells but contained less pronounced PHB granule staining than in *B. stylosanthis* and *Bradyrhizobium* sp. USDA3516 (**Fig. 4B**; **Fig. S3**). Bacteroids of *B. cajani* were slightly larger and wider than free-living cells but were unbranched, and SYTO9 intensity relative to free-living cells was higher than in *Bradyrhizobium* sp. USDA3516 (**Fig. 4C**; **Fig. S4**). Interestingly, bacteroids of *B. canariense* – the only ineffective symbiont to robustly form nodules – generally were branched and slightly larger than free-living cells, but these bacteroids had no increase in ploidy. This suggests that endoreduplication rather than branching is the most important aspect of the differentiation, at least within our strain set.

Bradyrhizobium sp. USDA 3516 genome properties

The apparent terminal differentiation of *Bradyrhizobium* sp. USDA3516 in *A. americana* was surprising, given that terminal differentiation was not observed in the effective Thai *A. americana* isolate *B.* sp. DOA9 [17]. To investigate whether this difference could be explained by the gene content of the two strains, we sequenced and assembled the *Bradyrhizobium* sp. USDA3516 genome. We found that the *Bradyrhizobium* sp. USDA3516 genome contains a single 7.8 Mbp chromosome with 7,283 ORFs predicted by both Prokka and Bakta prokaryotic annotation tools (**Fig. 5**). We did not detect any native plasmids in this strain; commonly *Bradyrhizobium* spp. do not encode symbiotic plasmids [21].

We annotated ORFs using the consensus from Bakta [22] and Prokka [23] annotation tools, InterPro protein domain analysis (for protein-coding ORFs) [24], and reciprocal best BLAST hit analysis against closely related and model bacterial strains (reference species are listed in the Methods; **Table S1**). These revealed the presence of well-known symbiosis-driving genes, including *nod* genes, indicating that this strain can produce Nod factors (**Fig. 5**). The strain appears to be metabolically versatile with multiple respiratory terminal electron acceptors (*fix*/cbb3, *cox*/c1, and two *cyo*/bo3 operons), and though it contains a RuBisCo (*cbb*) gene cluster, it does not contain other genes for photosynthesis in bradyrhizobia [25]. It encodes at least three secretion systems (*gsp*/T2SS, *rhc*/T3SS, *trb*/T4SS) and pili biosynthesis genes (*ctp*/*tad*), as well as two large flagellar gene clusters (*fla*) and three chemotaxis operons (*che*). Based on synteny with other genomes from Rhizobiales/Hyphomicrobiales members, we predict that flagellar cluster *fla2* encodes lateral flagellar genes [26]. This organism also includes signature lipid species of *Bradyrhizobium* spp. and rhizobia, such as genes involved in the biosynthesis of hopanoid lipids (*hpn*) and the synthesis and addition of very long chain fatty acids to lipid A (*acpXL*).

Comparison of *B.* sp. USDA 3516 to other symbiotic *Bradyrhizobium* spp.

We next assembled a genome-wide phylogeny of *Bradyrhizobium* species representatives using bac120 alignments from the GTDB Toolkit (**Fig. 6**) [27]. As expected from the gene content, *Bradyrhizobium* sp. USDA3516 is not part of the clade containing photosynthetic bradyrhizobia or the *B. japonicum* clade, and instead it is more closely related to other productive *A. americana* symbionts from this study: *B. cajani*, *B. arachidis*, and *B. stylosanthis*. The strain's closest relatives are *B. yuanmingense* CCBAU 10071 and the Thai *A. americana* symbiont *B.* sp. DOA9, with which it shares >92% average nucleotide identity (**Fig. S9A**).

The degree of nucleotide conservation between *B.* sp. DOA9 and *Bradyrhizobium* sp. USDA3516 is surprising given their contrasting phenotypes regarding bacteroid differentiation. We initially hypothesized that they may have lower than average similarity within genes known to be involved in the differentiation process. However, protein phylogenetic trees of the NCR peptide importer BclA (the *Bradyrhizbium* spp. homolog of BacA in *S. meliloti*) [20] indicated that *Bradyrhizobium* sp. USDA3516 BclA is more similar to the *B.* sp. DOA9 BclA than to the BclA proteins from other species with branched *A. americana* bacteroids (**Fig. S9B**). We also analyzed the FtsZ protein in *Bradyrhizobium* sp. USDA3516, based on recent data demonstrating that FtsZ depletion in the Rhizobiales/Hyphomicrobiales is sufficient to induce branching [28], yet the FtsZ protein tree topology is likewise similar to the species relationships (**Fig. S9C**).

One distinction between *B.* sp. DOA9 and *Bradyrhizobium* sp. USDA3516 that is not captured by comparing conserved genomic loci is the presence of unique gene groups, and it is possible that bacteroid branching in *Bradyrhizobium* sp. USDA3516 is driven by genes that are not present in *B.* sp. DOA9. We used the Proteinortho tool [29] to identify orthologous gene groups (OGs) found in all species with branched bacteroids (*Bradyrhizobium* sp. USDA3516, *B. arachidis*, *B. stylosanthis*, and *B. canariense*) and in none of the non-branching species (*B.* sp. DOA9 and *B. cajani*) (**Fig. S9D**). This analysis yielded a list of 45 OGs (**Table 2**), which includes genes involved in LPS biosynthesis and DNA replication. Interestingly, seven of these OGs are part of a conserved gene cluster in that is adjacent to the MinCDE cell topology factors (**Fig. 7**). Though the Min system is not essential in rhizobia, misregulation of Min protein expression in *S. meliloti* can induce branching [30], potentially indicating that altered regulation of the MinCDE region is required for branched bacteroids.

MATERIALS & METHODS

Bacterial strain cultivation

Strain *Bradyrhizobium* sp. USDA3516 was obtained from the USDA ARS National Rhizobium Germplasm Collection, courtesy of Patrick Elia. *Bradyrhizobium* spp. ORS285 and BTAi1 were originally obtained from Eric Giraud (LSTM, Montpellier, France) and later gifted by Dianne Newman (Caltech). All other strains were purchased from the DSMZ-German Collection of Microorganisms and Cell Cultures.

All *Bradyrhizobium* spp. and *Sinorhizobium* spp. strains were streaked on rich AG medium agar plates (4.6 mM sodium gluconate, 6.6 mM arabinose, 1 g/L yeast extract, 6 mM NH4Cl, 5.6 mM MES, 5 mM HEPES, 1 mM Na2HPO4, 1.76 mM Na2SO4, 88 µM CaCl2, 25 µM FeCl3, and 0.73 mM MgSO4, pH 6.6) from 10% glycerol stocks. Plates were grown at 30°C for 4-5 days before colonies were inoculated into 10mL AG rich liquid media. These cultures were grown to exponential phase (OD_{600} = 0.4-0.8) at 30°C and 250 rpm prior to plant inoculation. For plant

inoculation, cultures were pelleted by centrifugation at 4000g in a spinning bucket centrifuge and resuspended to OD_{600} = 1.0 in fresh AG. During inoculation, 300 uL of OD_{600} = 1.0 resuspensions were added to each 30 mL *A. americana* culture tube.

A. americana cultivation

Aeschynomene americana seeds (Hancock Farm & Seed Company) were surface sterilized by 5-minute incubation in 95% ethanol, followed by 30-minute incubation with 10% bleach, followed by 5 washes in sterile water. The seeds were then plated on 1% water agar plates. Plates were sealed with parafilm, wrapped to prevent light exposure, and germinated at 30°C for 3 days. Germinated seedlings were rooted into 30 mL culture tubes filled with Buffered Nodulation Medium (BNM: 2 mM $CaCl_2$, 2 mM MES, 0.5 mM KH_2PO_4, 0.5 mM $MgSO_4$, 16 µM $ZnSO_4$, 50 µM H_3BO_3, 50µM $MnCl_2$, 1 µM Na_2MoO_4, 0.1 µM $CuSO_4$, 0.1 µM $CoCl_2$, 50 µM Na_2EDTA, 50 µM $FeSO_4$) buffered to pH 6.5 using KOH. Rooted *A. americana* were then moved to growth chambers held at 12h light/dark cycles at 30°C and 80% humidity for the duration of the experiment.

Acetylene reduction assays

Whole *A. americana* plants were moved into 30 mL Balch tubes with 1mL of sterile water. Balch tubes were plugged with rubber septa and sealed with aluminum crimp caps, after which 10% of the headspace was removed via syringe and 16G needle and replaced with acetylene gas (Airgas). Samples were incubated overnight under growing conditions before measurement of ethylene production by GC-MS as described [31].

Bacteroid extraction

Nodules were removed from roots and submerged in a 10% bleach solution for 5 minutes. Nodules were then washed three times with Bacteroid Extraction Buffer (BEB: 113.7mM Disodium Malate, 125 mM KCl, 50mM TES buffer) before homogenization with mortar and pestle in 5 mL of BEB. Samples were then centrifuged at 100g for 10 minutes to remove plant debris. Cleared supernatant was moved to a new tube, centrifuged at 1500 g for 20 minutes, and resuspended in 1 mL of ice-cold BEB. All subsequent steps were performed at 4°C with ice-cold buffers. The resuspension was gently added to the top of a freshly prepared Percoll gradient with 10 mL 85%/10 mL 60%/10 mL 45% Percoll layers. The sample was spun through the Percoll gradients 10,000g for 30 minutes, after which a band of concentrated bacteroids was visible. A 5 mL fraction containing this band was collected, diluted 1:10 in BEB, and then centrifuged at 1500g for 20 min. The bacteroid pellet was washed again in 5 mL BEB to remove residual Percoll, resuspended in PBS with 4% fresh paraformaldehyde, and fixed at 4°C overnight.

Fluorescence staining

Nodule semi-thin sections (100 µm thickness) were collected using a 7000 smz-2 vibratome (Campden Instruments). Nodule sections were stained and mounted for imaging as described [31]. For cultured samples, cells were grown to mid-exponential phase (OD_{600} = 0.6) and pelleted at 4000 x g for 30 minutes. Cell pellets were resuspended in PBS with 4% fresh paraformaldehyde and fixed at 4°C overnight. Fixed cultured cells and fixed

bacteroids prepared as above were stained for microscopy by incubating with 7.5 μM SYTO9 for 30 minutes then with 0.25 μg/mL FM 4-64 for 10 minutes or with 0.5 μg/mL Nile Red for 30 minutes, all in PBS.

Microscopy

Confocal fluorescence images of nodule cross-sections were taken using a Zeiss LSM980 confocal microscope using either a 40X/1.3 NA or 63X/1.4 NA objective. All images were collected using an Airyscan 2 detector with the following wavelength ranges for each dye: Calcofluor White, 405nm laser excitation and 422-477 nm emission; SYTO9, 488 nm excitation and 495-550 nm emission; Propidium Iodide, 561nm excitation and 607-735 nm emission.

For imaging bacteroids, SYTO9 and FM 4-64 fluorescence images were acquired using a Zeiss LSM980 confocal microscope with a 40X/1.3 NA objective. Images were collected using an Airyscan 2 detector with the following wavelength ranges for each dye: SYTO9, 488 nm excitation and 483-506 nm emission; FM 4-64, 514 nm excitation and 500-751 nm emission. Phase images with SYTO9 and Nile Red fluorescence were acquired using a Nikon Ti2 inverted epifluorescence microscope with a 40X/0.75 NA phase objective. The following wavelength ranges were used for each dye: SYTO9 – 488 nm excitation, GFP emission filter cube (502-538 nm); Nile Red – 561 nm excitation, Nikon TRITC emission cube (570-613 nm).

Flow cytometry

Cultured cells and bacteroids were prepared as described above, stained with 0.025 μM SYTO9 for 15 minutes in PBS, and fixed in 4% paraformaldehyde/PBS at 4°C overnight. Samples were washed three times in PBS and then diluted to 1:10 - 1:100 in 1 mL PBS, depending upon the sample density. Flow cytometry was performed on samples with an Attune Nxt Acoustic Focusing Cytometer rujning Attune Nxt Software v. 3.2.1526.0. Forward scattering was collected at 350V and SYTO9 intensities were collected at 450V using a 488 nm excitation and 500-560 nm emission filter. For each sample, 100,000 events were recorded. Analysis was performed using the FloJo software.

Genome sequencing and assembly

Bradyrhizobium sp. USDA3516 was grown at 29°C overnight in a modified arabinose-gluconate medium [32] with shaking. DNA was extracted from *Bradyrhizobium* sp. USDA3516 and prepared for Oxford Nanopore sequencing, following protocols previously described, with the exception that the Ligation Sequencing Kit V14 was used [33]. The *PathogenSurveillance* pipeline was used to automatically process and assemble reads, assess assembly quality, and annotate the genome sequence [34].

Manual genome analysis

Preliminary annotation of the *Bradyrhizobium* sp. USDA3516 genome was performed using Prokka version 1.14.5 (https://github.com/tseemann/prokka) [23] and Bakta version 1.11.4 (https://github.com/oschwengers/bakta) [22]. Protein-coding genes were annotated using the InterProScan command line tool (version 5.69-101.0, https://github.com/ebi-pf-team/interproscan) [24]. Genes homologous with selected reference genomes were identified through custom reciprocal best BLAST hit analysis scripts using *blastp* (https://www.ncbi.nlm.nih.gov/books/NBK279690/) with an e-value threshold of 1e-20. Reference genomes selected

for this analysis were *Bradyrhizobium* sp. ORS 278 (https://www.uniprot.org/taxonomy/114615), *Bradyrhizobium* BTAi1 (https://www.uniprot.org/taxonomy/288000), *Bradyrhizobium diazoefficiens* USDA110 (https://www.uniprot.org/taxonomy/224911), *Rhodopseudomonas palustris* BAA-98 (https://www.uniprot.org/taxonomy/258594), *Sinorhizobium meliloti* 1021 (https://www.uniprot.org/taxonomy/266834), *Caulobacter vibroides* (formerly *crescentus*) CB15N (https://www.uniprot.org/taxonomy/565050), *Bacillus subtilis* 168 (https://www.uniprot.org/taxonomy/224308), *Escherichia coli* K12 (https://www.uniprot.org/taxonomy/83333). Final gene annotations were made by majority-rule across the above preliminary annotation sources and reviewed manually. Chromosome and operon annotations were visualized using Proksee (https://proksee.ca/) [35].

Orthologous protein groups were identified using Proteinortho version 6.3.6 (https://gitlab.com/paulklemm_PHD/proteinortho) [29]. The following proteome accessions were used for comparison with *Bradyrhizobium* sp. USDA3516: *Bradyrhizobium arachidis* CCBAU 051107 (UniProt UP000594015), *Bradyrhizobium brasilense* R5 (UniProt UP001221546), *Bradyrhizobium* BTAi1 (UniProt UP000000246), *Bradyrhizobium cajani* 1010 (UniProt UP000449969), *Bradyrhizobium canariense* BTA-1 (UniProt UP000887172), *Bradyrhizobium diazoefficiens* USDA110 (UniProt UP000002526), *Bradyrhizobium* sp. DOA9 (NCBI RefSeq GCF_000617845.2), *Bradyrhizobium elkanii* USDA 76 (NCBI Assembly GCA_023278185.1), *Bradyrhizobium japonicum* USDA 6 (UniProt UP000005663), *Bradyrhizobium* sp. ORS 285 (UniProt UP000196578), *Bradyrhizobium semiaridum* WSM 1704 (NCBI Assembly GCA_020329505.1), *Bradyrhizobium stylosanthis* (UniProt UP000319949).

Phylogenetic tree reconstruction

For the *Bradyrhizobium* species tree, a bac120 alignment of *Bradyrhizobium* species representatives from the Genome Taxonomy Database (GTDB) was generated using GTDB Toolkit v2.4.0+ (gtdb-tk, https://github.com/Ecogenomics/GTDBTk) [27]. For protein trees, sequences were aligned using the MUSCLE v. 5.1 sequence alignment program (https://www.drive5.com/muscle/muscle.html) [36]. Maximum likelihood trees were generated using IQ-TREE 2 (https://iqtree.github.io/) [37]. The optimal nucleotide substitution model for each alignment was determined by ModelFinder [38] and 1,000 replicates were used to calculate branch support values using ultrafast bootstrap approximation (UFBoot) [39]. Trees were visualized and annotated using TreeViewer (https://treeviewer.org/) [40].

DISCUSSION

A. americana is a basal, diploid member of the Dalbergioids with potential use as a genetic model for Nod factor-dependent Dalbergioid symbiosis. Here we evaluated the symbiont range of *A. americana* from central Florida and characterized a nodule isolate from the same region, *Bradyrhizobium* sp. USDA3516, which appears to be a close relative of the effective Thai *A. americana* symbiont *B.* sp DOA9. We find that *A. americana* is effectively nodulated by diverse non-native *Bradyrhizobium* strains but is not compatible with non-photosynthetic strains, consistent with earlier work. Microscopy of nodule cross-sections and isolated bacteroids revealed that most of the compatible symbionts of *A. americana* exhibit hallmarks of terminal bacteroid differentiation (branched morphologies and higher ploidy than cultured cells), albeit to varying degrees across symbiont species.

What is the role of morphological changes in bacteroids? Different jointvetch species induce distinct symbiont morphologies, including both elongated (*A. afraspera [8]* and *A. fluminensis [41]*) and spherical bacteroids (*A. evenia [42]* and *A. indica [8]*), and whether these morphological differences affect symbiotic efficiency is unclear. Prior studies by Lamouche *et al.* [43, 44] attempted to address this question by inoculating the same set of *Bradyrhizobium* strains (*Bradyrhizobium* sp. ORS285, ORS287, ORS335, and ORS357) onto three jointvetch hosts: two species that induce spherical bacteroids (*A. evenia* and *A. indica*) and one species with elongated bacteroids (*A. afraspera*). The authors then quantified the benefit conferred to each plant by each symbiont via the increase in plant biomass relative to the nodule biomass – a proxy for the benefit to the host relative to the host's investment in symbiosis. Using this metric, the two jointvetches inducing spherical bacteroids were consistently observed to receive greater benefits from the same strains than the jointvetch with elongated bacteroids. Based on this, the authors concluded that spherical bacteroids may be inherently more effective than elongated bacteroids.

Our study contradicts the view that bacteroid morphology *per se* is a major determinant of symbiotic efficiency. Within the same host, we identified symbionts with four distinct bacteroid phenotypes: (i) branching only, (ii) elevated ploidy only, (iii) both branching and elevated ploidy, and (iv) neither branching nor elevated ploidy. We found that branching alone was not sufficient for a strain to function as an effective symbiont, whereas elevated ploidy was observed in all effective strains. Though the effective symbionts that we identified do not provide a large enough sample size to suggest that higher bacteroid ploidy is strictly necessary for effective *A. americana* symbiosis, we can conclude that branched bacteroid morphologies are not required, a conclusion that is also supported by the effective interaction between *A. americana* and the non-branching bacteroids of *B.* sp. DOA9 [9].

The disagreement between this work and Lamouche *et al.* has several potential explanations. Our groups employ different metrics for evaluating symbiosis (proportion of non-nodule biomass conferred vs. acetylene reduction), and the significance of bacteroid morphological changes may differ between *A. americana* and the other jointvetches examined. However, we note that Lamouche *et al.* rely on comparison across rather than within jointvetch species, and that species-specific differences in symbiotic mechanisms beyond morphological changes may account for the symbiosis efficiencies in spherical bacteroid- vs. elongated bacteroid-producing hosts. Ultimately, a careful examination of bacteroid morphotype relevance will require generating symbiont strains lacking only the factors required for bacteroid branching, which could then be assayed in a single host-symbiont context.

Currently we do not know what genetic factors regulate morphological and/or ploidy changes in *A. americana* bacteroids, nor in those of most other Dalbergioid legumes. *A. americana* presumably produces NCR peptides, and the presence of branched bacteroids likely relates to the degree of compatibility between *A. americana* NCRs and the presence or sequence of a symbiont's cell cycle control factors. Others have found that disruption of the cell division factor FtsZ in species of Hyphomicrobiales/Rhizobiales order is sufficient to induce branched cells in culture [28], as is overexpression of Min proteins *Sinorhizobium meliloti* (where Min proteins are non-essential) [30]. It is curious, then, that we identified a *minCDE*-adjacent operon that is conserved in all *A. americana* symbionts with branched bacteroids, though the function of these genes – and whether they affect Min protein levels – is unknown. This provides the foundation for future work to determine whether *A. americana* indeed produces NCR peptides, what these peptides target, and whether the conserved *minCDE* genomic region is relevant to bacteroid differentiation.

DECLARATIONS

Ethics approval and consent to participate

Not applicable.

Consent for publication

Not applicable.

Availability of data and materials

Bradyrhizobium sp. USDA3615 genome will be made available on NCBI upon acceptance for publication.

Competing interests

The authors have no competing interests to declare.

Funding

Funding for this project was provided by the Carnegie Institution for Science Endowment to B.J.B. Pilot experiments were performed by students in the Marine Biological Laboratory's Molecular & Cell Biology of Symbiosis course, which is funded by a grant from the Gordon & Betty Moore Foundation.

Author contributions

T.S.C., A.A.A., and A.S. performed *A. americana* inoculation experiments and bacteroid analyses. J.R.S. sequenced and assembled the *Bradyrhizobium* sp. USDA3516 genome. C.P.R., R.A.B., J.H.C., and B.J.B. analyzed the *Bradyrhizobium* sp. USDA3516 genome. B.J.B. designed the project, acquired funding, and prepared the manuscript.

Acknowledgements

We thank Will Ludington (Johns Hopkins University) for Attune flow cytometry access and members of the Ludington lab for training and technical assistance. Members of the Belin lab provided helpful discussions of the manuscript, and Mahmud Siddiqi (Carnegie) provided technical assistance for microscopy. We are grateful to Carnegie Embryology's IT, front office, and facilities support staff for making our work possible.

TABLES

Symbiont Strain	Host Species	Host Common Name	Host Tribe
Bradyrhizobium sp USDA3516	*Aeschynomene americana*	American jointvetch	Dalbergioid
Bradyrhizobium sp ORS285	*Aeschynomene afraspera*	African jointvetch	Dalbergioid
Bradyrhizobium BTAi1^{T}	*Aeschynomene indica*	Indian jointvetch	Dalbergioid
Bradyrhizobium arachidis LMG26975^{T}	*Arachis hypogaea*	Peanut	Dalbergioid
Bradyrhizobium stylosanthis BR10^{T}	*Stylosanthes guianensis*	Stylo	Dalbergioid
Bradyrhizobium diazoefficiens USDA110^{T}	*Glycine max*	Soybean	Milletioid
Bradyrhizobium japonicum USDA6^{T}	*Glycine max*	Soybean	Milletioid
Bradyrhizobium elkanii USDA76^{T}	*Glycine max*	Soybean	Milletioid
Sinorhizobium fredii NGR234^{T}	*Glycine max*	Soybean	Milletioid
Bradyrhizobium cajani AMBPC1010^{T}	*Cajanus cajan*	Pigeon pea	Milletioid
Sinorhizobium fredii HH103^{T}	*Lablab purpureus*	Hyacinth bean	Milletioid
Bradyrhizobium semiaridium LMG31654^{T}	*Tephrosia gardneri*	Hoarypea	Milletioid
Bradyrhizobium brasilense R ^{T}	*Vigna unguiculata*	Cowpea	Milletioid
Bradyrhizobium canariense BTA-1^{T}	*Cytisus proliferus*	Tagasaste	Genistoid

Table 1. **Strains of rhizobia used for *A. americana* inoculation**. Collection of strains used for inoculation of *A. americana* in this study, including the scientific and common names of the host from which each strain was isolated and the legume tribe to which the host belongs. '^{T}' indicates type strains.

Locus	Gene	Description
Brady3516_00244		**SsuA/THI5-like domain-containing protein**
Brady3516_00245		**TetR family transcriptional regulator, NicS type**
Brady3516_00246		**ABC transporter type 1, MetI-like superfamily**
Brady3516_00247		**NAD(P)-binding domain superfamily**
Brady3516_00248		**GNAT family N-acetyltransferase, YitH/HolE-like**
Brady3516_00249		**DapA-like protein**
Brady3516_00250		**Aliphatic sulfonates import ATP-binding protein SsuB-like**
Brady3516_00266		Ribonuclease Z/Hydroxyacylglutathione hydrolase-like metallo-beta-lactamase
Brady3516_00760		Hypothetical protein
Brady3516_01459		DUF6636 domain containing protein
Brady3516_01628		AMP-dependent synthetase/ligase
Brady3516_02047		NAD(P)-dependent dehydrogenase, short-chain alcohol dehydrogenase family
Brady3516_02208	*fsr*	Fosmidomycin resistance protein
Brady3516_02463		Hypothetical protein
Brady3516_02636		AMP-dependent synthetase/ligase
Brady3516_03010		Hypothetical protein
Brady3516_03026		ABC-type multidrug transport system, ATPase component
Brady3516_03502		Hypothetical protein
Brady3516_03543		Hypothetical protein
Brady3516_03544		CHRD domain-containing protein
Brady3516_03546		Cyclic di-GMP phosphodiesterase
Brady3516_03565		Hypothetical protein
Brady3516_03575		Acetyltransferase, LpxA superfamily
Brady3516_03623		Multidrug transporter EmrE superfamily, Amino Acid and Vitamin Transporters
Brady3516_03703		Transmembrane protein TauE-like
Brady3516_03873		Bordetella uptake gene
Brady3516_04043		Epoxide hydrolase-like
Brady3516_04171		ABC-type molybdate transport system, periplasmic Mo-binding protein ModA
Brady3516_04290		Hypothetical protein
Brady3516_04336	*pcaC_3*	4-carboxymuconolactone decarboxylase/NDH-1 regulator
Brady3516_05191		Hypothetical protein
Brady3516_05329		DUF1236 domain-containing protein
Brady3516_06440		Hypothetical protein
Brady3516_06649	*rfbC*	dTDP-4-dehydrorhamnose 3,5-epimerase
Brady3516_06662		Acetyltransferase, LpxA superfamily
Brady3516_06663		DegT/DnrJ/EryC1/StrS family aminotransferase
Brady3516_06686		Hypothetical protein
Brady3516_06716		L-2-Haloacid dehalogenase
Brady3516_06994		YjbJ superfamily
Brady3516_07077	*traF*	Type IV secretory pathway, protease TraF
Brady3516_07079	*repA*	Replication initiator protein A
Brady3516_07080		DNA-binding protein
Brady3516_07083		YspA, cpYpsA-related SLOG domain protein
Brady3516_07084		TOPRIM domain protein

Table 2. Orthologous gene groups (OGs) specific to species with branched bacteroids in *A. americana*. OGs identified in all species that form branched bacteroids in *A. americana* (*Bradyrhizobium* sp. USDA3516, *B. arachidis*, *B. stylosanthis*, and *B. canariense*) and in none of the non-branching species (*B.* sp. DOA9 and *B. cajani*). OGs are indicated by their locus ID in *Bradyrhizobium* sp. USDA3516, which their corresponding gene names and descriptions assigned by Bakta. Genes highlighted in bold correspond to the conserved operon shown in Figure 7.

FIGURES

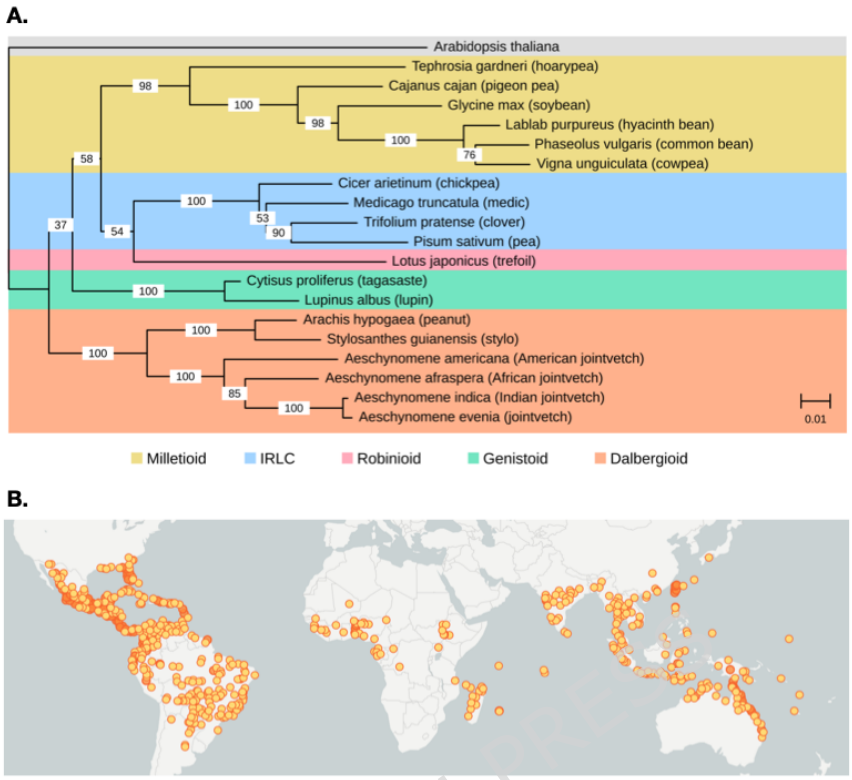

Figure 1. **Selected tribes of the *Papillionideae***. (**A**) Maximum likelihood phylogenetic tree of select legume species based on conserved regions of *matK* sequences; color coding indicates corresponding legume tribes. Scale bar indicates substitutions per 1000 nucleotides. Numbers at mid-branch points (highlighted in white) indicate branch support values using ultrafast bootstrap approximation (UFBoot), based on 1000 bootstraps: 100 = highest confidence, 0 = no confidence. *Arabidopsis thaliana* was used as the outgroup. (**B**) Geographic distribution of *Aeschynomene americana* (Legume Data Portal, Accessed Sept. 2025).

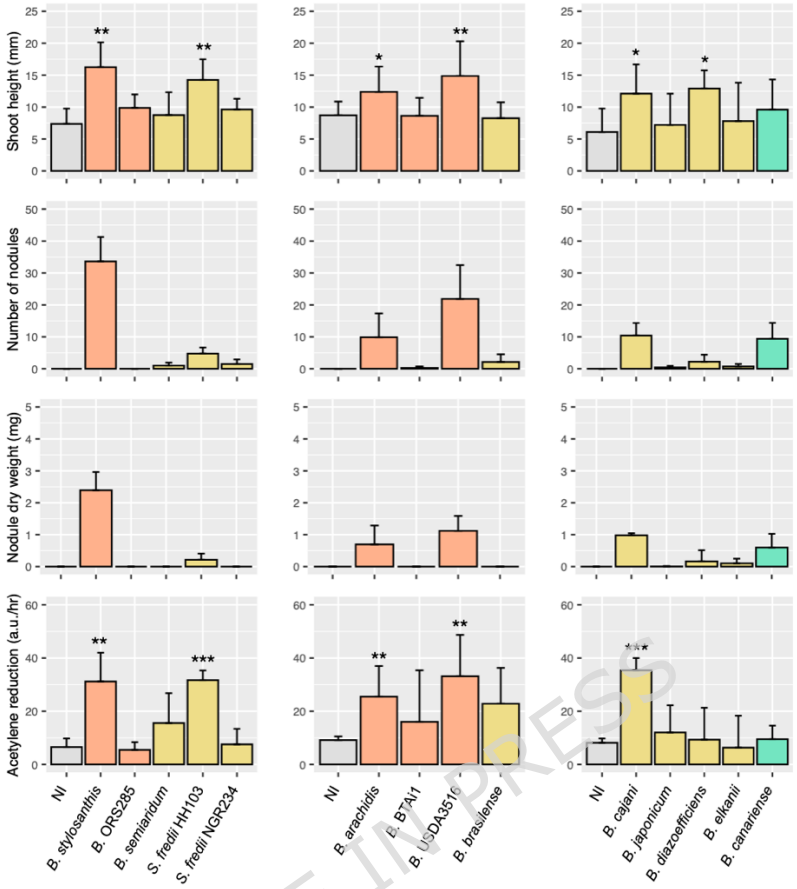

Figure 2. *A. americana* growth is promoted by non-photosynthetic Dalbergioid symbionts. Average shoot height, nodule number, nodule dry weight, and acetylene reduction activity for *A. americana* plants inoculated with each strain from Table 1. (N=7-9 plants per condition; 'NI' = non-inoculated). Error bars indicate standard deviation. Colors of bars indicate native host tribe, according to the legend in Figure 1. Asterisks indicate p-values from two-tailed t-test comparison with non-inoculated plants: '*' < 0.01, '**' < 0.001, '***', < 0.0001.

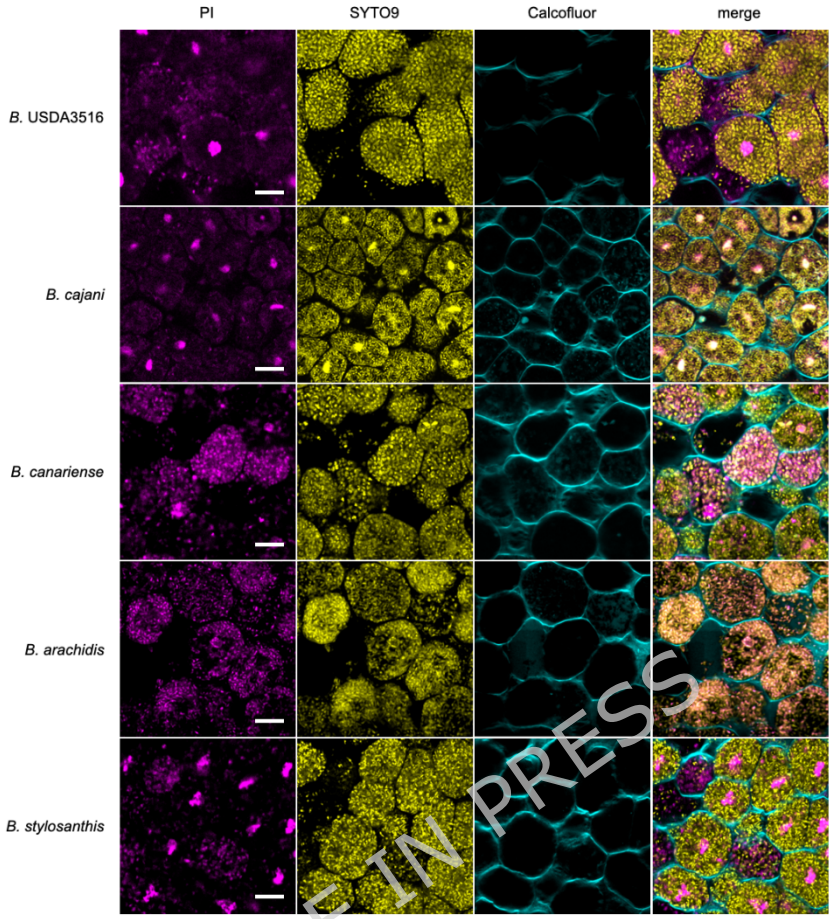

Figure 3. ***A. americana*** **bacteroids are terminally differentiated.** Representative confocal images of nodule cross-sections from *A, americana* plants inoculated with strains of bradyrhizobia indicated in row labels. Sections were collected at 14 dpi and stained with Calcofluor (cyan), SYTO9 (yellow), and propidium iodide ("PI"; magenta). Scale bars = 10 microns.

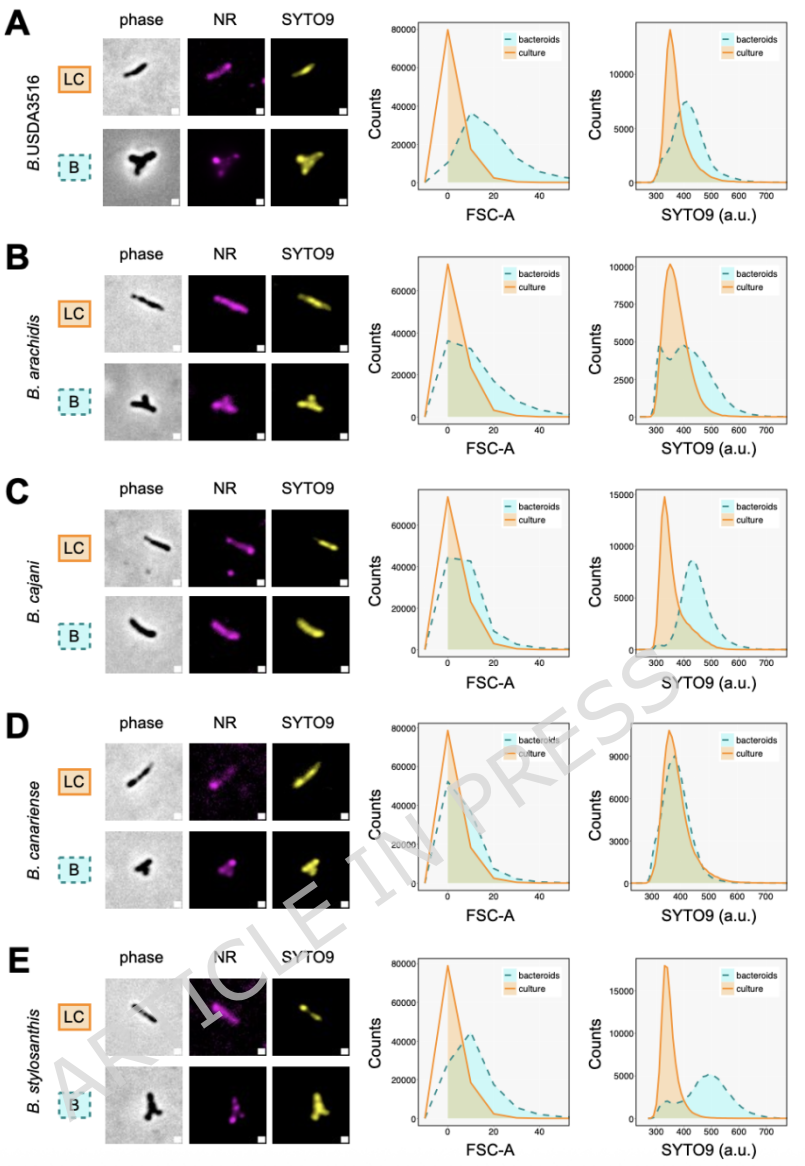

Figure 4. Productive bacteroids exhibit higher levels of endoreduplication. Representative phase and fluorescence images (*left*) with flow cytometry forward scatter distributions (*center)* and SYTO9 intensity distributions (*right*) for *A. americana* bacteroids ("B", dotted blue filled lines) versus cultured cells ("LC", solid orange filled line) after staining with Nile Red (NR) and SYTO9: (**A**) *Bradyrhizobium sp. USDA3516*, (**B**) *B. arachidis*, (**C**) *B. cajani*, (**D**) *B. canariense*, (**E**) *B. stylosanthis*. Scale bars indicate 1 micron.

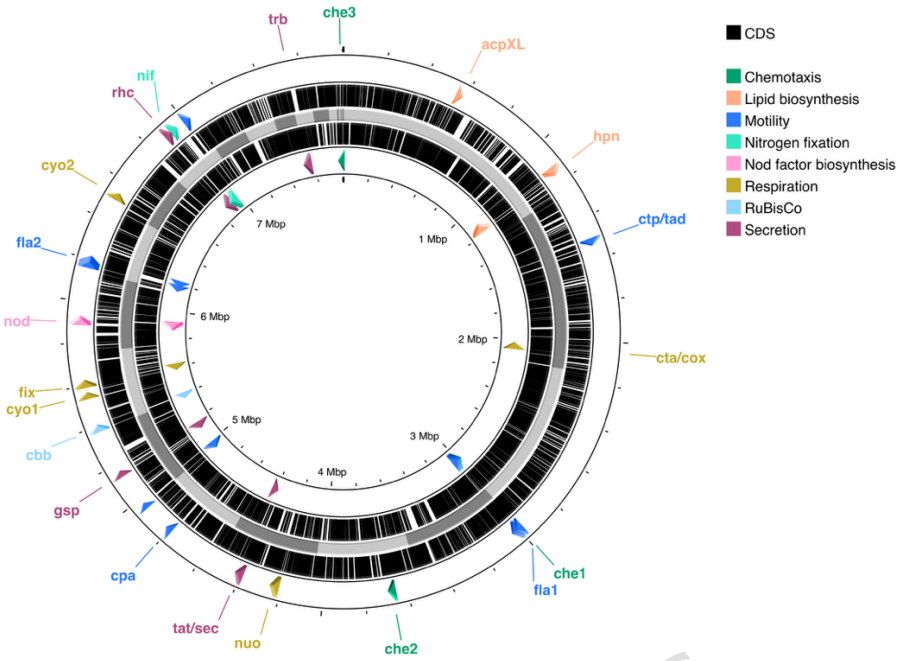

Figure 5. Genome architecture of native *A. americana* symbiont *Bradyrhizobium sp. USDA3516.* Genome architecture of *Bradyrhizobium* sp. USDA3516 consisting of a single circular chromosome. Inner ring (alternating grey regions) denotes individual scaffolds. Second rings from center indicate positions of protein-coding genes (CDS, in black) as annotated in Table S1. Outermost rings from center indicate ORFs for symbiotically relevant gene categories, as denoted in the legend. Illustration generated using Proksee (https://proksee.ca/)[35].

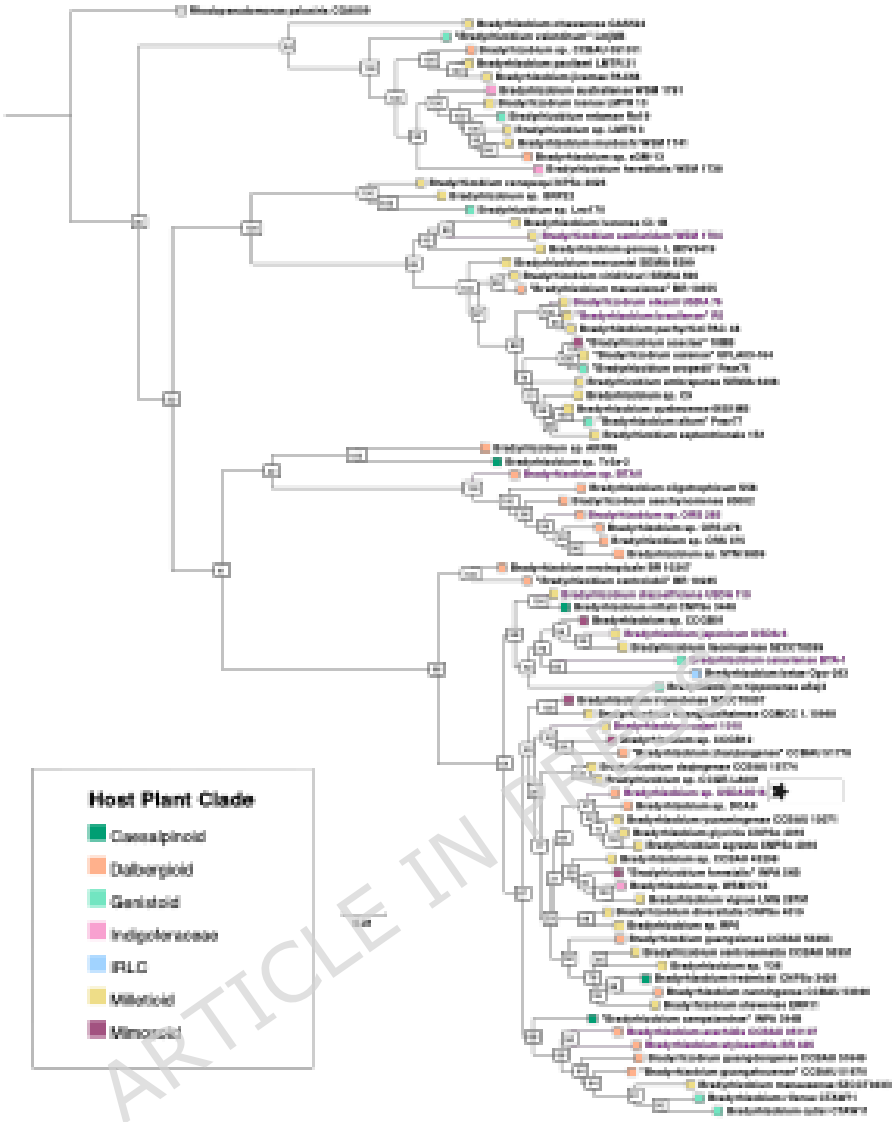

Figure 6. Bac120 species tree of representative *Bradyrhizobium* spp. Maximum likelihood tree for conserved regions across select *Bradyrhizobium* species representatives; informal species names that are not accepted by LPSN are indicated with quotation marks. Branch names for species used for *A. americana* inoculation in this study are highlighted in purple, and the *Bradyrhizobium* sp. USDA3516 genome is indicated with a black star. Colored boxes at branch tips indicate the legume clade (tribe/subfamily) of the host species from which the strain was originally isolated (see Legend). Numbers at internal nodes (highlighted in white) indicate branch support values using ultrafast bootstrap approximation (UFBoot), based on 1000 bootstraps: 100 = highest confidence, 0 = no confidence. The outgroup sequence is indicated with a grey branch tip label. Scale bar indicates substitutions per 1000 nucleotides.

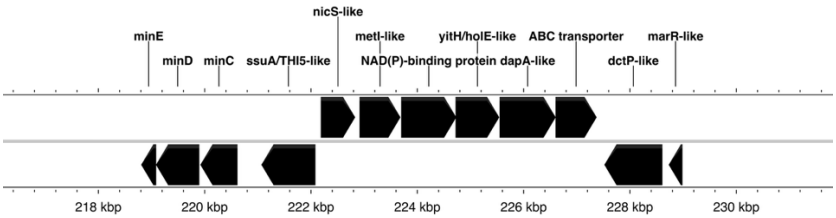

Figure 7. **Conserved operon adjacent to *minCDE* found in all species of bradyrhizobia that form branched bacteroids in *A. americana*.** Illustration generated using Proksee (https://proksee.ca/)[35].

SUPPLEMENTAL DATA

Table S1. Manually curated gene annotations in *Bradyrhizobium* sp. USDA3516. Information provided in each column follows: (A) Ordered locus ID, (B) Contig, (C-D) Start and stop nucleotide positions, relative to the contig; (E) Coding strand (+ or -); (F) Preferred gene names, where available; (G) Consensus gene description; (H) Prokka suggested gene name; (I) Prokka suggested gene description; (J) Bakta suggested gene name; (K) Bakta suggested gene description; (L) InterPro domains identified by Interproscan, formatted as Domain ID:Domain Name; (M) Gene name of reciprocal best BLAST hit (RBBH) from *Bradyrhizobium* sp. ORS 278, when present; (N) Gene description of RBBH from *Bradyrhizobium* sp. ORS 278, when present; (O) Gene name of RBBH from *Bradyrhizobium* BTAi1, when present; (P) Gene description of RBBH from *Bradyrhizobium* BTAi1, when present; (Q) Gene name of RBBH from *Bradyrhizobium diazoefficiens* USDA110, when present; (R) Gene description of RBBH from *Bradyrhizobium diazoefficiens* USDA110, when present; (S) Gene name of RBBH from *Rhodopseudomonas palustris* BAA-98, when present; (T) Gene description of RBBH from *Rhodopseudomonas palustris* BAA-98, when present; (U) Gene name of RBBH from *Sinorhizobium meliloti* 1021, when present; (V) Gene description of RBBH from *Sinorhizobium meliloti* 1021, when present; (W) Gene name of RBBH from *Caulobacter vibroides* (formerly *crescentus*) CB15N, when present; (X) Gene description of RBBH from *Caulobacter vibroides* (formerly *crescentus*) CB15N, when present; (Y) Gene name of RBBH from *Bacillus subtilis* 168, when present; (Z) Gene description of RBBH from *Bacillus subtilis* 168, when present; (AA) Gene name of RBBH from *Escherichia coli* K12, when present; (BB) Gene description of RBBH from *Escherichia coli* K12, when present.

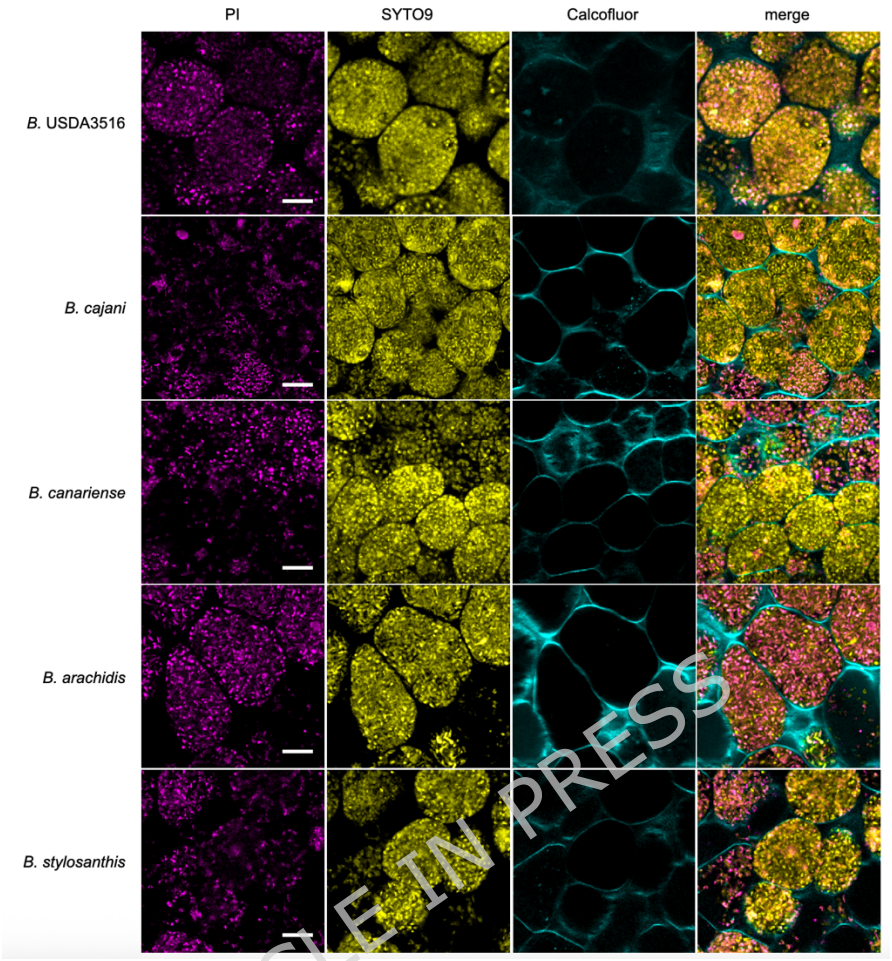

Figure S1. Representative confocal images of *A. americana* nodule cross-sections collected at 35 dpi. Sections were stained with Calcofluor (cyan), SYTO9 (yellow), and propidium iodide ("PI"; magenta). Scale bars = 10 microns.

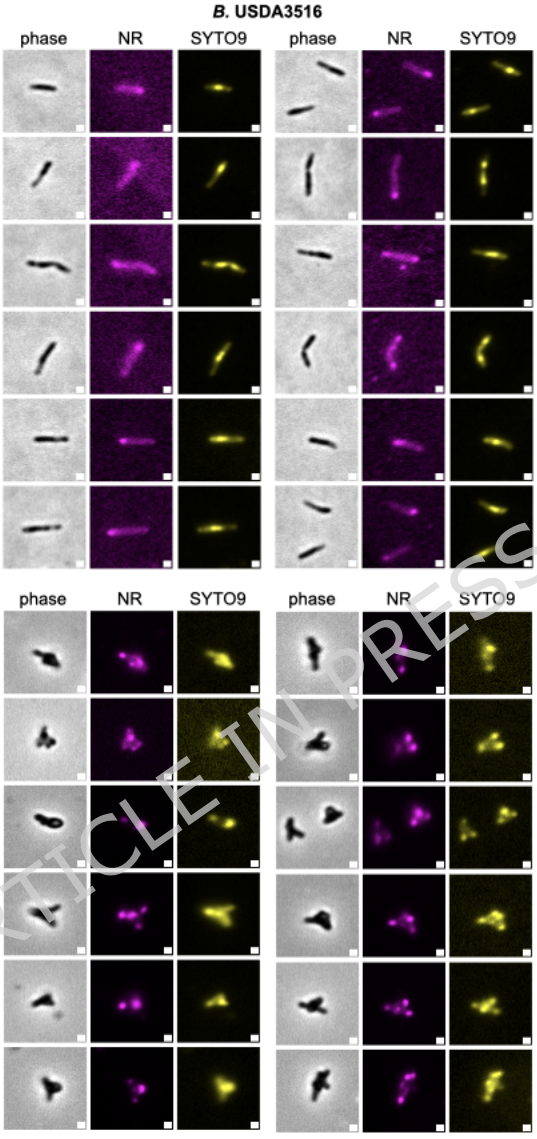

Figure S2. Additional phase and fluorescence images for *Bradyrhizobium* sp. USDA3516 bacteroids and cultured cells stained with Nile Red (NR) and SYTO9. Scale bars indicate 1 micron.

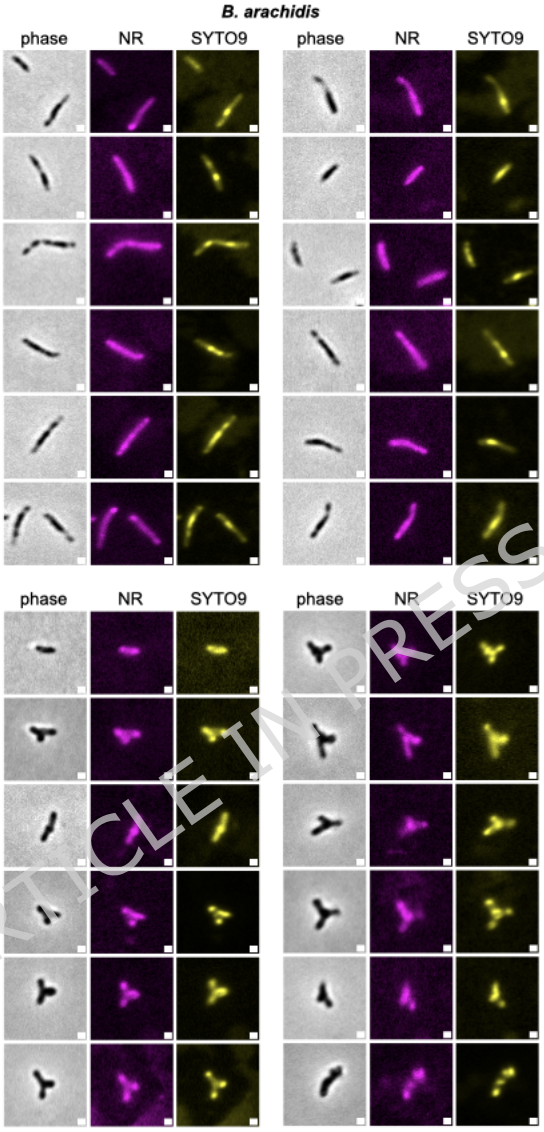

Figure S3. Additional phase and fluorescence images for *B. arachidis* bacteroids and cultured cells stained with Nile Red (NR) and SYTO9. Scale bars indicate 1 micron.

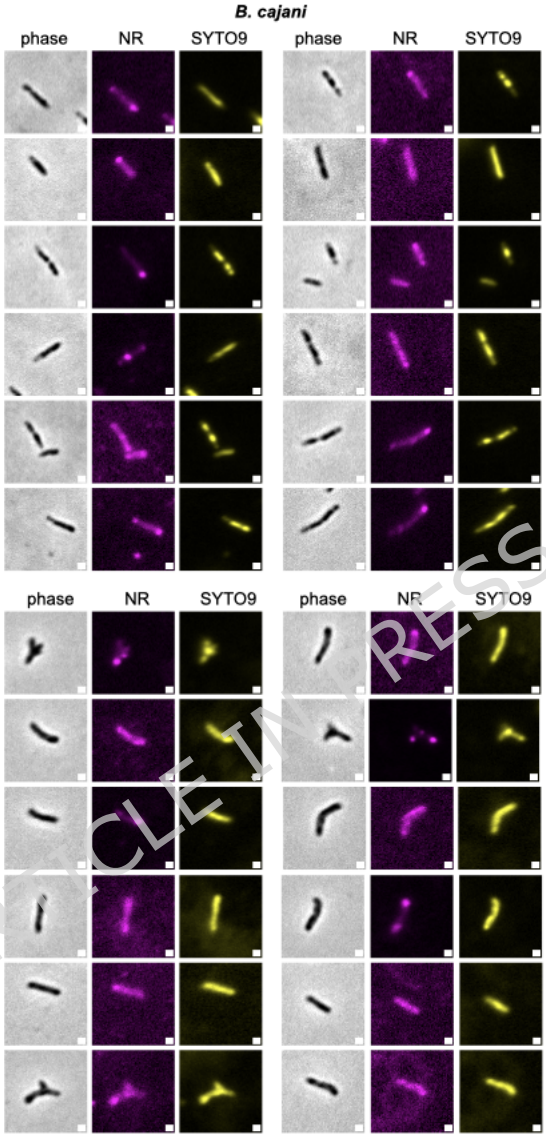

Figure S4. Additional phase and fluorescence images for *B. cajani* bacteroids and cultured cells stained with Nile Red (NR) and SYTO9. Scale bars indicate 1 micron.

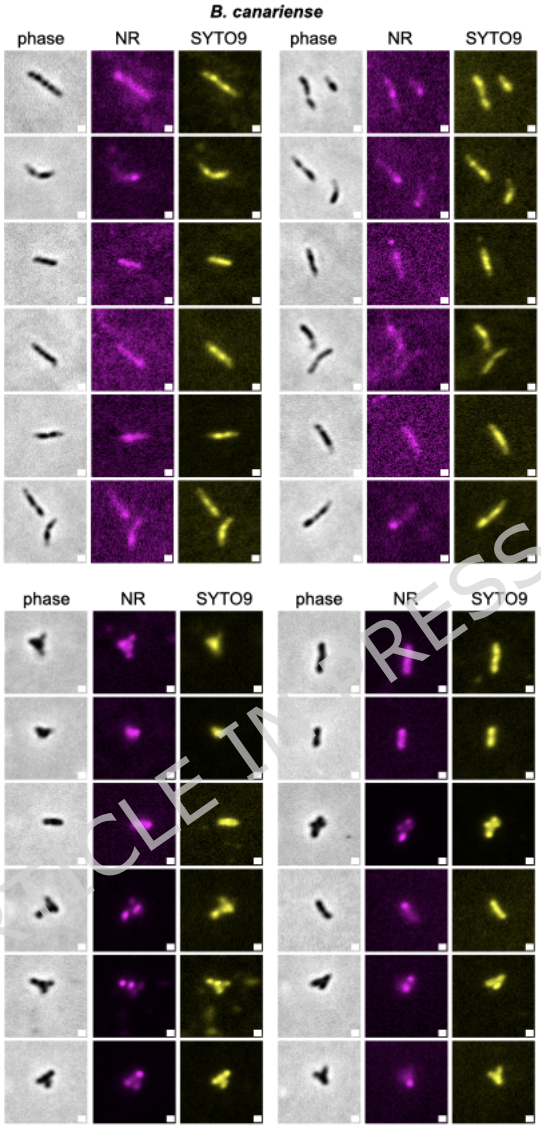

Figure S5. Additional phase and fluorescence images for *B. canariense* bacteroids and cultured cells stained with Nile Red (NR) and SYTO9. Scale bars indicate 1 micron.

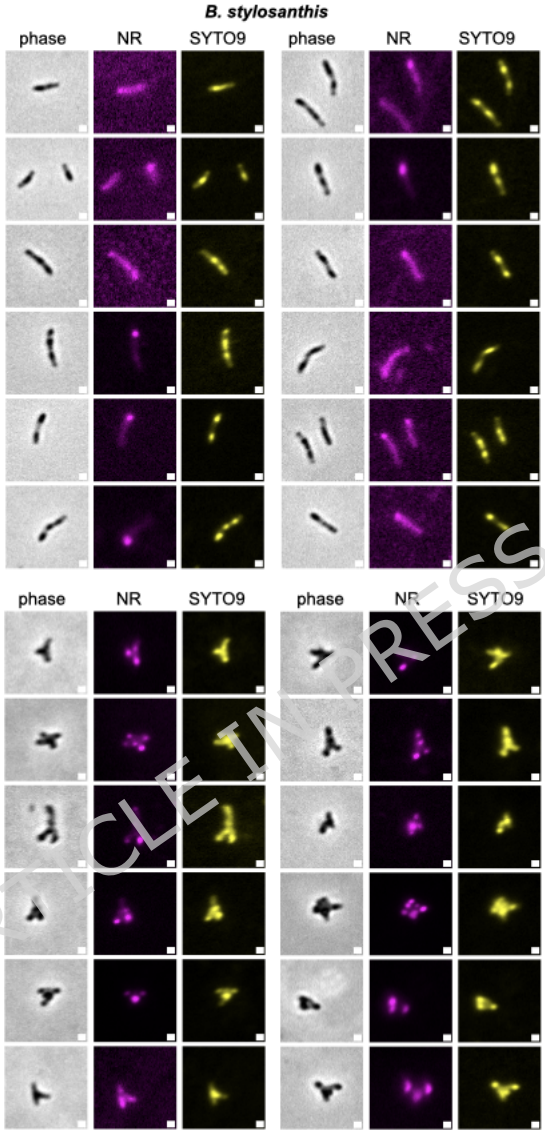

Figure S6. Additional phase and fluorescence images for *B. stylosanthis* bacteroids and cultured cells stained with Nile Red (NR) and SYTO9. Scale bars indicate 1 micron.

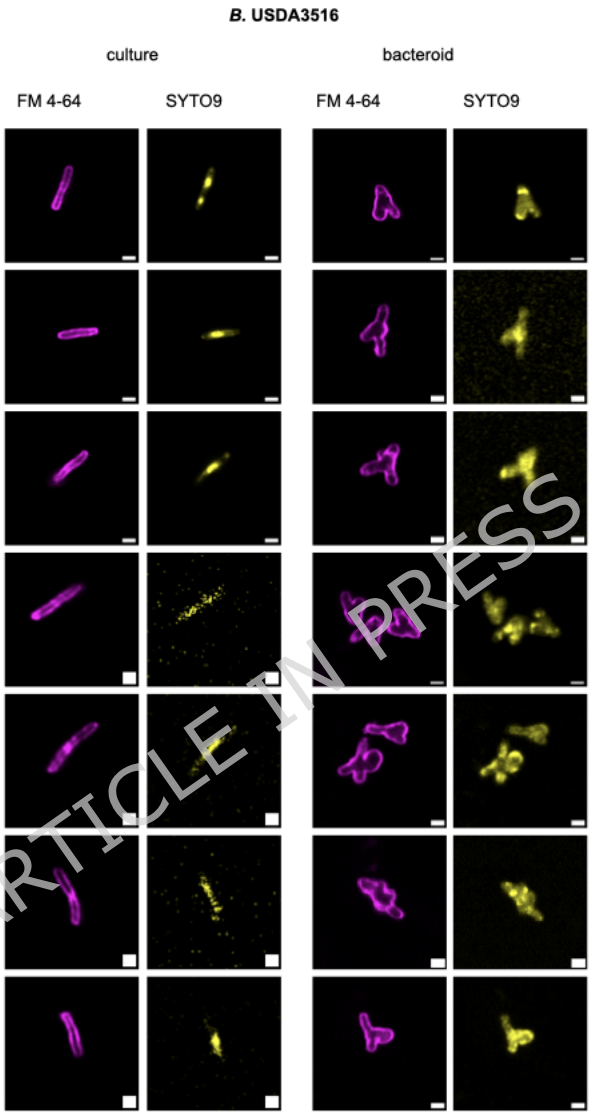

Figure S7. Airyscan superresolution imaging of *Bradyrhizobium* sp. USDA3516 bacteroids and cultured cells stained with FM 4-64 and SYTO9. Scale bars indicate 1 micron.

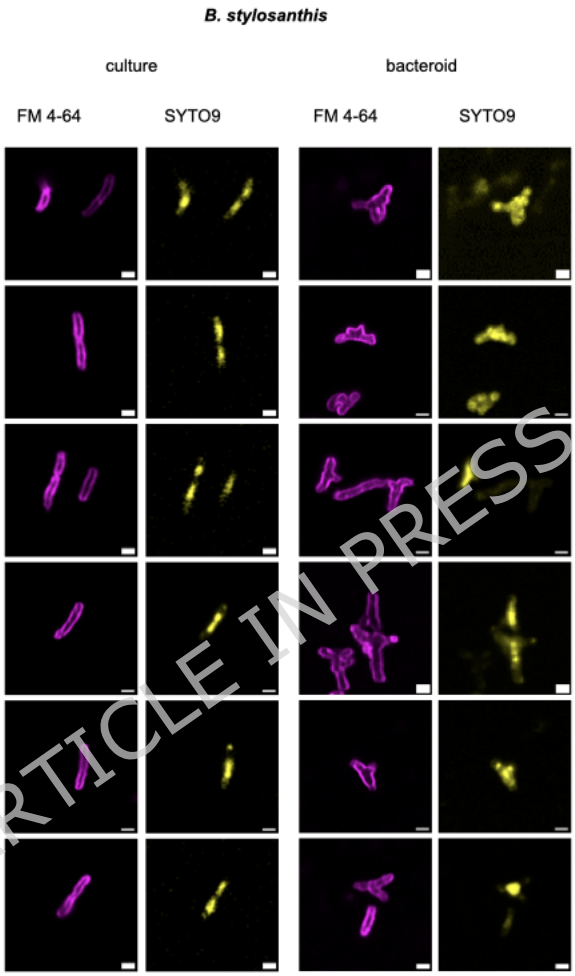

Figure S8. Airyscan superresolution imaging of *B. stylosanthis* bacteroids and cultured cells stained with FM 4-64 and SYTO9. Scale bars indicate 1 micron.

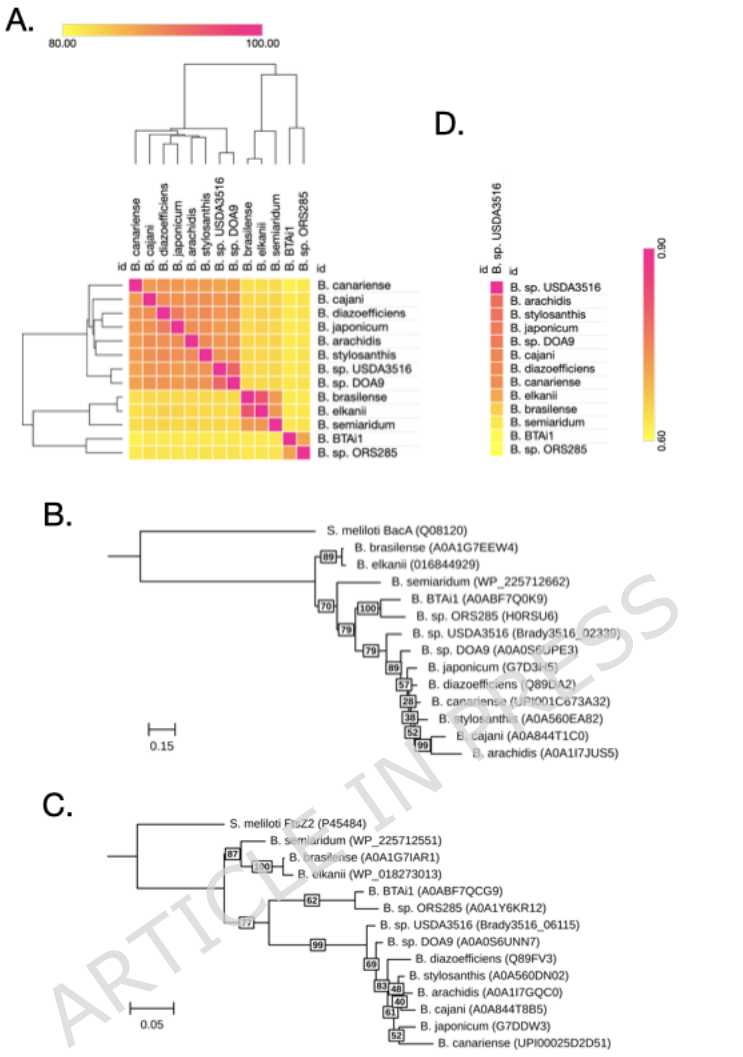

Figure S9. (**A**) Heatmap of average nucleotide identity across stains used for *A. americana* inoculation and *B.* sp. DOA9. Calculated with FastANI v. 1.34 (https://github.com/ParBLiSS/FastANI) [45] and visualized with Morpheus (https://software.broadinstitute.org/morpheus/) (**B-C**) Maximum likelihood phylogenetic tree of BclA (**B**) and FtsZ (**C**) homologs from genomes in (A). Numbers at internal nodes (highlighted in white) indicate branch support values using ultrafast bootstrap approximation (UFBoot), based on 1000 bootstraps: 100 = highest confidence, 0 = no confidence. UniProt IDs are provided in parentheses in the branch labels. Outgroup sequences are *S. meliloti* homologs. Scale bars indicate substitutions per 1000 amino acids. (**D**) Heatmap illustrating the percentage of orthologous gene groups (OGs) shared between *B.* sp. 3516 and all other strains in (A).

REFERENCES

1. Legume Phylogeny Working Group (LPWG) A, G. C., Atahuachi Burgos, M., Bagnatori Sartori, Â. L., Balan, A., Bandyopadhyay, S., Barbosa Pinto, R., Barrett, R., Boatwright, J. S., Borges, L. M., Bortoluzzi, R., Broich, S. L., Brullo, S., Bruneau, A., Cardinal-McTeague, W., Cardoso, D., Castro Silva, I. C., Cervantes, A., Choo, L. M., et al. : **The World Checklist of Vascular Plants (WCVP): Fabaceae**: Royal Botanic Gardens, Kew, Richmond, UK; 2025.
2. Wojciechowski M, Lavin M, Sanderson M: **A phylogeny of legumes (Leguminosae) based on analyses of the plastid matK gene resolves many well-supported subclades within the family**. *American Journal of Botany* 2004, **91**(11):1846–1862.
3. Pessi G, Ahrens C, Rehrauer H, Lindemann A, Hauser F, Fischer H, Hennecke H: **Genome-wide transcript analysis of Bradyrhizobium japonicum bacteroids in soybean root nodules**. *Molecular Plant-Microbe Interactions* 2007, **20**(11):1353–1363.
4. Guerra-Garcia F, Sankari S: **NCR peptides in plant-bacterial symbiosis: applications and importance**. *Trends in Microbiology* 2025, **33**(2):147–150.
5. Nations FAOotU: **Agricultural production statistics 2010–2023**. In: *FAOSTAT Analytical Briefs.* Rome, Italy; 2024: 16.
6. Giraud E, Moulin L, Vallenet D, Barbe V, Cytryn E, Avarre J, Jaubert M, Simon D, Cartieaux F, Prin Y *et al*: **Legumes symbioses:: Absence of Nod genes in photosynthetic bradyrhizobia**. *Science* 2007, **316**(5829):1307–1312.
7. Guha S, Molla F, Sarkar M, Ibañez F, Fabra A, DasGupta M: **Nod factor-independent 'crack-entry' symbiosis in dalbergoid legume Arachis hypogaea**. *Environmental Microbiology* 2022, **24**(6):2732–2746.
8. Bonaldi K, Gargani D, Prin Y, Fardoux J, Gully D, Nouwen N, Goormachtig S, Giraud E: **Nodulation of Aeschynomene afraspera and A. indica by Photosynthetic Bradyrhizobium Sp. Strain ORS285: The Nod-Dependent Versus the Nod-Independent Symbiotic Interaction**. *Molecular Plant-Microbe Interactions* 2011, **24**(11):1359–1371.
9. Noisangiam R, Teamtisong K, Tittabutr P, Boonkerd N, Toshiki U, Minamisawa K, Teaumroong N: **Genetic Diversity, Symbiotic Evolution, and Proposed Infection Process of Bradyrhizobium Strains Isolated from Root Nodules of Aeschynomene americana L. in Thailand**. *Applied and Environmental Microbiology* 2012, **78**(17):6236–6250.
10. Czernic P, Gully D, Cartieaux F, Moulin L, Guefrachi I, Patrel D, Pierre O, Fardoux J, Chaintreuil C, Nguyen P *et al*: **Convergent Evolution of Endosymbiont Differentiation in Dalbergioid and Inverted Repeat-Lacking Clade Legumes Mediated by Nodule-Specific Cysteine-Rich Peptides**. *Plant Physiology* 2015, **169**(2):1254–1265.
11. Gully D, Czernic P, Cruveiller S, Mahé F, Longin C, Vallenet D, François P, Nidelet S, Rialle S, Giraud E *et al*: **Transcriptome Profiles of Nod Factor-independent Symbiosis in the Tropical Legume Aeschynomene evenia**. *Scientific Reports* 2018, **8**.
12. Raul B, Bhattacharjee O, Ghosh A, Upadhyay P, Tembhare K, Singh A, Shaheen T, Ghosh A, Torres-Jerez I, Krom N *et al*: **Microscopic and Transcriptomic Analyses of Dalbergoid Legume Peanut Reveal a Divergent Evolution Leading to Nod-Factor-Dependent Epidermal Crack-Entry and Terminal Bacteroid Differentiation**. *Molecular Plant-Microbe Interactions* 2022, **35**(2):131–145.
13. Boukherissa A, Sankari S, Timchenko T, Bourge M, Mergaert P, diCenzo GC, Shykoff JA, Alunni B, Rodríguez de la Vega RC: **Structure-based phylogenetic analysis reveals multiple events of convergent evolution of cysteine-rich antimicrobial peptides in legume-rhizobium symbiosis**. *bioRxiv* 2025:2025.2009.2009.675119.
14. Quilbé J, Lamy L, Brottier L, Leleux P, Fardoux J, Rivallan R, Benichou T, Guyonnet R, Becana M, Villar I *et al*: **Genetics of nodulation in Aeschynomene evenia uncovers mechanisms of the rhizobium-legume symbiosis**. *Nature Communications* 2021, **12**(1).
15. Chaintreuil C, Gully D, Hervouet C, Tittabutr P, Randriambanona H, Brown S, Lewis G, Bourge M, Cartieaux F, Boursot M *et al*: **The evolutionary dynamics of ancient and recent polyploidy in the African semiaquatic species of the legume genus Aeschynomene**. *New Phytologist* 2016, **211**(3):1077–1091.
16. Brottier L, Chaintreuil C, Simion P, Scornavacca C, Rivallan R, Mournet P, Moulin L, Lewis G, Fardoux J, Brown S *et al*: **A phylogenetic framework of the legume genus Aeschynomene for comparative genetic analysis of the Nod-dependent and Nod-independent symbioses**. *Bmc Plant Biology* 2018, **18**.
17. Teamtisong K, Songwattana P, Noisangiam R, Piromyou P, Boonkerd N, Tittabutr P, Minamisawa K, Nantagij A, Okazaki S, Abe M *et al*: **Divergent Nod-Containing Bradyrhizobium sp DOA9 with a Megaplasmid and its Host Range**. *Microbes and Environments* 2014, **29**(4):370–376.

18. Okazaki S, Noisangiam R, Okubo T, Kaneko T, Oshima K, Hattori M, Teamtisong K, Songwattana P, Tittabutr P, Boonkerd N *et al*: **Genome Analysis of a Novel Bradyrhizobium sp DOA9 Carrying a Symbiotic Plasmid**. *Plos One* 2015, **10**(2).
19. Grant W, Trese A: **Developmental regulation of nodulation in Arachis hypogea (peanut) and Aeschynomene americana (jointvetch)**. *Symbiosis* 1996, **20**(3):247–258.
20. Guefrachi I, Pierre O, Timchenko T, Alunni B, Barrière Q, Czernic P, Villaécija-Aguilar J, Verly C, Bourge M, Fardoux J *et al*: **Bradyrhizobium BclA Is a Peptide Transporter Required for Bacterial Differentiation in Symbiosis with Aeschynomene Legumes**. *Molecular Plant-Microbe Interactions* 2015, **28**(11):1155–1166.
21. Weisberg A, Sachs J, Chang J: **Dynamic Interactions Between Mega Symbiosis ICEs and Bacterial Chromosomes Maintain Genome Architecture**. *Genome Biology and Evolution* 2022, **14**(6).
22. Schwengers O, Jelonek L, Dieckmann M, Beyvers S, Blom J, Goesmann A: **Bakta: rapid and standardized annotation of bacterial genomes via alignment- free sequence identification**. *Microbial Genomics* 2021, **7**(11).
23. Seemann T: **Prokka: rapid prokaryotic genome annotation**. *Bioinformatics* 2014, **30**(14):2068–2069.
24. Jones P, Binns D, Chang H, Fraser M, Li W, McAnulla C, McWilliam H, Maslen J, Mitchell A, Nuka G *et al*: **InterProScan 5: genome-scale protein function classification**. *Bioinformatics* 2014, **30**(9):1236–1240.
25. Mornico D, Miché L, Béna G, Nouwen N, Verméglio A, Vallenet D, Smith A, Giraud E, Médigue C, Moulin L: **Comparative Genomics of Aeschynomene Symbionts: Insights into the Ecological Lifestyle of Nod-Independent Photosynthetic Bradyrhizobia**. *Genes* 2012, **3**(1):35–61.
26. Garrido-Sanz D, Redondo-Nieto M, Mongiardini E, Blanco-Romero E, Durán D, Quelas J, Martin M, Rivilla R, Lodeiro A, Althabegoiti M: **Phylogenomic Analyses of Bradyrhizobium Reveal Uneven Distribution of the Lateral and Subpolar Flagellar Systems, Which Extends to Rhizobiales**. *Microorganisms* 2019, **7**(2).
27. Chaumeil P-A, Mussig AJ, Hugenholtz P, Parks DH: **GTDB-Tk v2: memory friendly classification with the genome taxonomy database**. *Bioinformatics* 2022, **38**(23):5315–5316.
28. Aubry B, Randich A, Hudson B, Horton E, Brown PJB: **Ancient Truncated FtsZ Paralogs Likely Tune Cell Division in Hyphomicrobiales**. *bioRxiv* 2025:2025.2009.2029.679267.
29. Klemm P, Stadler P, Lechner M: **Proteinortho6: pseudo-reciprocal best alignment heuristic for graph-based detection of (co-)orthologs**. *Frontiers in Bioinformatics* 2023, **3**.
30. Cheng J, Sibley C, Zaheer R, Finan T: **A Sinorhizobium meliloti minE mutant has an altered morphology and exhibits defects in legume symbiosis**. *Microbiology-Sgm* 2007, **153**:375–387.
31. Pan H, Shim A, Lubin M, Belin B: **Hopanoid lipids promote soybean-Bradyrhizobium symbiosis**. *Mbio* 2024, **15**(4).
32. Sachs JL, Kembel SW, Lau AH, Simms EL: **In Situ Phylogenetic Structure and Diversity of Wild Bradyrhizobium Communities**. *Applied and Environmental Microbiology* 2009, **75**(14):4727–4735.
33. Weisberg AJ, Rahman A, Backus D, Tyavanagimatt P, Chang JH, Sachs JL: **Pangenome Evolution Reconciles Robustness and Instability of Rhizobial Symbiosis**. *mBio* 2022, **13**(3):e00074–00022.
34. Foster ZSL, Sudermann MA, Parada Rojas CH, Blair LK, Iruegas Bocardo F, Dhakal U, Weisberg AJ, Phan H, Chang JH, Grunwald NJ: **PathogenSurveillance: an automated pipeline for population genomic analyses and pathogen identification**. *bioRxiv* 2025:2025.2010.2031.685798.
35. Grant J, Enns E, Marinier E, Mandal A, Herman E, Chen C, Graham M, Van Domselaar G, Stothard P: **Proksee: in-depth characterization and visualization of bacterial genomes**. *Nucleic Acids Research* 2023, **51**(W1):W484–W492.
36. Edgar RC: **MUSCLE: multiple sequence alignment with high accuracy and high throughput**. *Nucleic Acids Research* 2004, **32**(5):1792–1797.
37. Minh BQ, Schmidt HA, Chernomor O, Schrempf D, Woodhams MD, von Haeseler A, Lanfear R: **IQ-TREE 2: New Models and Efficient Methods for Phylogenetic Inference in the Genomic Era**. *Molecular Biology and Evolution* 2020, **37**(5):1530–1534.
38. Kalyaanamoorthy S, Minh BQ, Wong TKF, von Haeseler A, Jermiin LS: **ModelFinder: fast model selection for accurate phylogenetic estimates**. *Nature Methods* 2017, **14**(6):587–589.
39. Hoang DT, Chernomor O, von Haeseler A, Minh BQ, Vinh LS: **UFBoot2: Improving the Ultrafast Bootstrap Approximation**. *Molecular Biology and Evolution* 2017, **35**(2):518–522.
40. Bianchini G, Sánchez-Baracaldo P: **TreeViewer: Flexible, modular software to visualise and manipulate phylogenetic trees**. *Ecology and Evolution* 2024, **14**(2).

41. Loureiro MF, James EK, Sprent JI, Franco AA: **Stem and root nodules on the tropical wetland legume Aeschynomene fluminensis**. *New Phytol* 1995, **130**(4):531–544.
42. Fabre S, Gully D, Poitout A, Patrel D, Arrighi JF, Giraud E, Czernic P, Cartieaux F: **Nod Factor-Independent Nodulation in Aeschynomene evenia Required the Common Plant-Microbe Symbiotic Toolkit**. *Plant Physiol* 2015, **169**(4):2654–2664.
43. Lamouche F, Gully D, Chaumeret A, Nouwen N, Verly C, Pierre O, Sciallano C, Fardoux J, Jeudy C, Szucs A *et al*: **Transcriptomic dissection of Bradyrhizobium sp. strain ORS285 in symbiosis with Aeschynomene spp. inducing different bacteroid morphotypes with contrasted symbiotic efficiency**. *Environmental Microbiology* 2019, **21**(9):3244–3258.
44. Lamouche F, Bonadé-Bottino N, Mergaert P, Alunni B: **Symbiotic Efficiency of Spherical and Elongated Bacteroids in the Aeschynomene-Bradyrhizobium Symbiosis**. *Frontiers in Plant Science* 2019, **10**.
45. Jain C, Rodriguez-R LM, Phillippy AM, Konstantinidis KT, Aluru S: **High throughput ANI analysis of 90K prokaryotic genomes reveals clear species boundaries**. *Nature Communications* 2018, **9**(1):5114.

A.

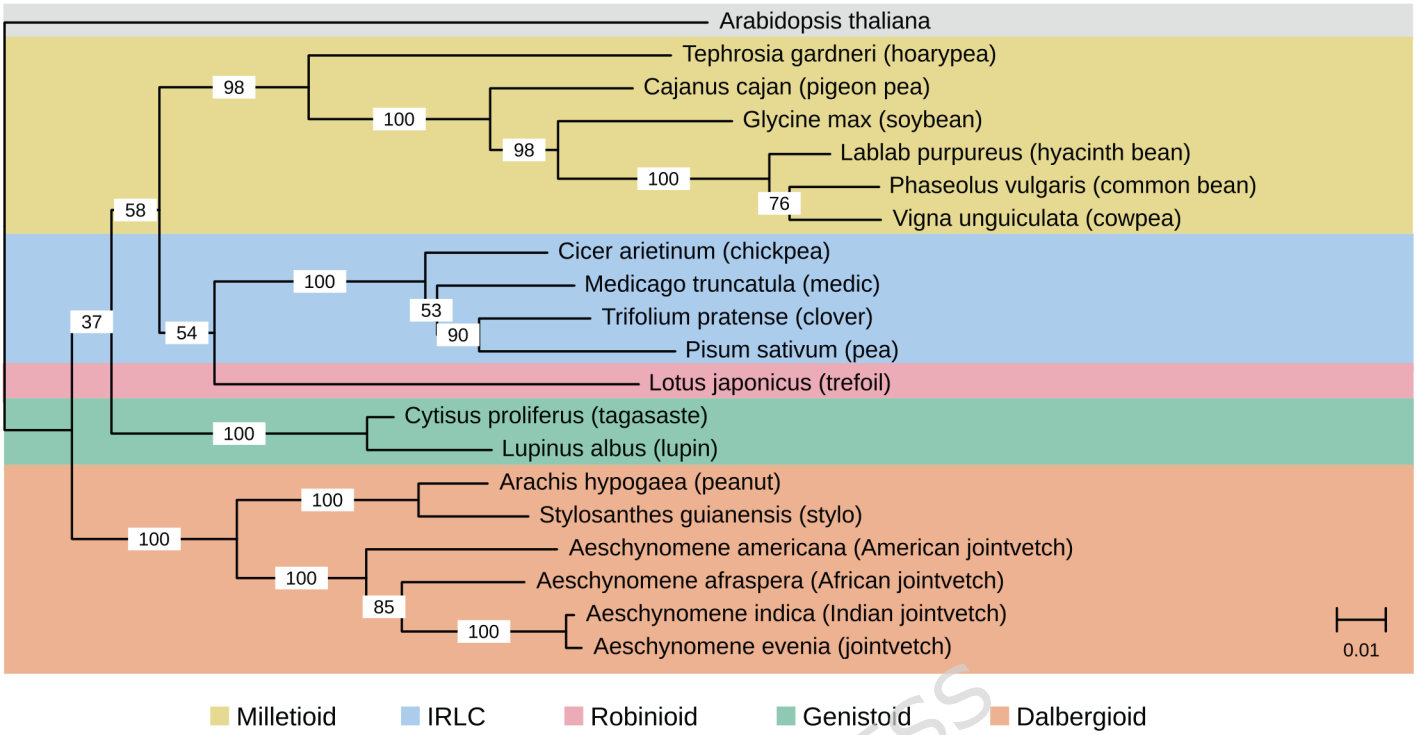

B.